# Current Clamp and Modeling Studies of Low-Threshold Calcium Spikes in Cells of the Cat's Lateral Geniculate Nucleus

X. J. ZHAN,[1] C. L. COX,[1] J. RINZEL,[2] AND S. MURRAY SHERMAN[1]
[1]*Department of Neurobiology, State University of New York, Stony Brook, 11794-5230; and* [2]*Center for Neural Science and Courant Institute of Mathematical Sciences, New York University, New York, New York 10003*

**Zhan, X. J., C. L. Cox, J. Rinzel, and S. Murray Sherman.** Current clamp and modeling studies of low-threshold calcium spikes in cells of the cat's lateral geniculate nucleus. *J. Neurophysiol.* 81: 2360–2373, 1999. All thalamic relay cells display a voltage-dependent low-threshold $Ca^{2+}$ spike that plays an important role in relay of information to cortex. We investigated activation properties of this spike in relay cells of the cat's lateral geniculate nucleus using the combined approach of current-clamp intracellular recording from thalamic slices and simulations with a reduced model based on voltage-clamp data. Our experimental data from 42 relay cells showed that the actual $Ca^{2+}$ spike activates in a nearly all-or-none manner and in this regard is similar to the conventional $Na^+/K^+$ action potential except that its voltage dependency is more hyperpolarized and its kinetics are slower. When the cell's membrane potential was hyperpolarized sufficiently to deinactivate much of the low-threshold $Ca^{2+}$ current ($I_T$) underlying the $Ca^{2+}$ spike, depolarizing current injections typically produced a purely ohmic response when subthreshold and a full-blown $Ca^{2+}$ spike of nearly invariant amplitude when suprathreshold. The transition between the ohmic response and activated $Ca^{2+}$ spikes was abrupt and reflected a difference in depolarizing inputs of $<1$ mV. However, activation of a full-blown $Ca^{2+}$ spike was preceded by a slower period of depolarization that was graded with the amplitude of current injection, and the full-blown $Ca^{2+}$ spike activated when this slower depolarization reached a sufficient membrane potential, a quasithreshold. As a result, the latency of the evoked $Ca^{2+}$ spike became less with stronger activating inputs because a stronger input produced a stronger depolarization that reached the critical membrane potential earlier. Although $Ca^{2+}$ spikes were activated in a nearly all-or-none manner from a given holding potential, their actual amplitudes were related to these holding potentials, which, in turn, determined the level of $I_T$ deinactivation. Our simulations could reproduce all of the main experimental observations. They further suggest that the voltage-dependent $K^+$ conductance underlying $I_A$, which is known to delay firing in many cells, does not seem to contribute to the variable latency seen in activation of $Ca^{2+}$ spikes. Instead the simulations indicate that the activation of $I_T$ starts initially with a slow and graded depolarization until enough of the underling transient (or T) $Ca^{2+}$ channels are recruited to produce a fast, ''autocatalytic'' depolarization seen as the $Ca^{2+}$ spike. This can produce variable latency dependent on the strength of the initial activation of T channels. The nearly all-or-none nature of $Ca^{2+}$ spike activation suggests that when a burst of action potentials normally is evoked as a result of a $Ca^{2+}$ spike and transmitted to cortex, this signal is largely invariant with the amplitude of the input activating the relay cell.

## INTRODUCTION

One of the most important cellular properties exhibited by thalamic relay neurons is a voltage-dependent, transient, low-threshold $Ca^{2+}$ conductance, leading to depolarization via $Ca^{2+}$ entry through T-type $Ca^{2+}$ channels (Crunelli et al. 1987; Jahnsen and Llinás 1984a,b). This $Ca^{2+}$ current thus is known as $I_T$, and it produces a low-threshold spike referred to here as the ''$Ca^{2+}$ spike.'' $I_T$ can be activated by a depolarizing input, such as an excitatory postsynaptic potential (EPSP), but only if the membrane already has been hyperpolarized sufficiently for $\geq$50–100 ms (Jahnsen and Llinás 1984a). This is because at more depolarized potentials, $I_T$ is *inactivated* and a period of hyperpolarization is required to remove the inactivation or *deinactivate* $I_T$. In regard to its transient nature, the low-threshold $Ca^{2+}$ conductance underlying $I_T$ behaves much like the $Na^+$ conductance underlying the conventional action potential except the voltage sensitivity of $I_T$ operates in a more hyperpolarized range and its kinetics are slower.

The importance of $I_T$ derives from the fact that the large, depolarizing $Ca^{2+}$ spike that it produces usually reaches threshold for activating conventional $Na^+/K^+$ action potentials, producing a brief burst of firing (Jahnsen and Llinás 1984a,b). This is known as the *burst mode* of firing and reflects the response of a relay cell to depolarizing inputs when the cell is initially hyperpolarized. When the cell is depolarized initially so that $I_T$ is inactive, the cell responds to the same depolarizing inputs with a steady stream of unitary action potentials, and this is known as the *tonic mode* of firing (Huguenard and McCormick 1992; Jahnsen and Llinás 1984a,b; McCormick and Huguenard 1992b; Steriade and Llinás 1988). Both firing modes are a ubiquitous property of relay cells throughout the mammalian thalamus, and both firing modes have been seen during both in vitro and in vivo recording, the latter including recording from awake, behaving animals (Ghazanfar and Nicolelis 1997; Guido and Weyand 1995; Guido et al. 1992, 1995; Sherman and Guillery 1996). It is now clear that the different patterns of firing represented by burst and tonic firing provide different types of relays of information to cortex. Because the firing mode is determined by the inactivation state of $I_T$ at the time an activating, depolarizing input, such as an EPSP, arrives at a relay cell, it is of great interest to understand how $I_T$ behaves.

Since the first descriptions of $I_T$ and burst firing in thalamic neurons, which involved intracellular recording in current-clamp mode (Jahnsen and Llinás 1984a,b), much of the quantitative and systematic study of $I_T$ has involved voltage-clamp recording, often in acutely dissociated cells and usually in rodents (Coulter et al. 1989; Hernández-Cruz and Pape 1989). The main advantage of this approach is that it permits a more complete description of the voltage dependency and kinetics of a voltage-dependent conductance, such as that associated with

The costs of publication of this article were defrayed in part by the payment of page charges. The article must therefore be hereby marked ''*advertisement*'' in accordance with 18 U.S.C. Section 1734 solely to indicate this fact.

 

$I_T$. Such data have enabled the development of Hodgkin-Huxley-like models that reproduce many properties of $Ca^{2+}$ spikes (Crunelli et al. 1989; Destexhe et al. 1998; Huguenard and McCormick 1992, 1994; McCormick and Huguenard 1992; Wang et al. 1991; Williams et al. 1997). However, among those aspects that have not been studied systematically in current-clamp mode, experimentally and including comparison with theory, is the nature of threshold for $Ca^{2+}$-spike generation.

The main purpose of the present study is to do this for relay cells of the lateral geniculate nucleus, the thalamic relay of retinal input to cortex, using current-clamp recording from in vitro slice preparations. We have found that the sensitivity for generation of $Ca^{2+}$ spikes is surprisingly high, with nearly all-or-none threshold behavior, and that these spikes and their associated bursts of action potentials occur with quite long latency near threshold. We compare our experimental data with simulations from a cellular model based on published voltage-clamp data. Also, our recordings are from the cat thalamus and the model is derived from voltage-clamp studies of rodent thalamus, so our comparisons also serve to test the generality of the behavior of $I_T$ across species.

## METHODS

### *Slice preparation*

All intracellular recordings were made from relay neurons of the cat's lateral geniculate nucleus in an in vitro thalamic slice preparation. Young animals (4–8 wk old) of either sex were handled in compliance with approved animal protocols. Briefly, animals were anesthetized deeply with a mixture of ketamine (25 mg/kg) and xylazine (2 mg/kg) and mounted in a stereotaxic device. We then opened a rectangular area of skull overlying the lateral geniculate nucleus and removed a block of tissue containing the lateral geniculate nucleus. After placing this block in oxygenated cold slicing solution (see next section), we killed the animal with an overdose of pentobarbital sodium. Thalamic slices (400–500 $\mu$m thick) were cut in a coronal or sagittal plane with a vibrating tissue slicer and placed in a holding chamber for $\geq$2 h before recording. Individual slices were transferred to an interface type recording chamber and continuously superfused with warm oxygenated physiological solution (see next section). The tissue was maintained at 33°C for all recordings.

### *Solutions*

The slicing solution was used throughout the tissue preparation until the slice was transferred to the holding chamber. It contained (in mM) 2.5 KCl, 1.25 $NaH_2PO_4$, 10.0 $MgCl_2$, 0.5 $CaCl_2$, 26.0 $NaHCO_3$, 11.0 glucose, and 234.0 sucrose. The physiological solution used in the holding and recording chamber for intracellular recording contained (in mM) 126.0 NaCl, 2.5 KCl, 1.25 $NaH_2PO_4$, 2.0 $MgCl_2$, 2.0 $CaCl_2$, 26.0 $NaHCO_3$, and 10.0 glucose; and it was gassed with a mixture of 95% $O_2$-5% $CO_2$ to a final pH of 7.4. In some experiments, the $Na^+$ channel blocker, tetrodotoxin (TTX; 0.5–1 $\mu$M), was added to the bath to block conventional $Na^+/K^+$ action potentials. The intracellular recording electrodes were filled with a solution that was either 3 M KAc or 1 M KAc with 2–5% neurobiotin.

### *Electrophysiological recordings and data analysis*

We obtained intracellular recordings in current-clamp mode from the geniculate relay cells using sharp electrodes. Recording electrodes were pulled to an impedance of 40–80 M$\Omega$ at 100 Hz when filled with the aforementioned solution. An Axoclamp 2A amplifier was used in bridge mode to enable current-clamp recordings. During the recordings, we adjusted an active bridge circuit to balance the drop in potential produced by passing current through the recording electrode. Current protocols were generated using either AxoData or pClamp on a laboratory computer, and the data were stored digitally with a temporal resolution of 0.2 ms. Cells were held at different initial holding potentials by injecting current into the cell (i.e., the holding current). The duration of holding current before evoking responses assured that any depolarizing sag due to $I_h$ would reach an equilibrium, leading to a stable membrane voltage for a sufficient time to create a stable level of $I_T$ inactivation. Responses, including $Ca^{2+}$ spikes, then were evoked by depolarizing current steps on top of the initial holding current, the steps ranging from 10 to 3,000 pA and having a duration of 200–1,000 ms. After >10 s of holding current, additional current steps were given on top of the holding current at a rate ranging from 0.1 to 0.3 Hz to ensure a stable initial holding potential before the depolarizing steps.

We adopted a set of minimum requirements to judge an intracellular recording as acceptable. These included having a resting membrane potential more negative than −50 mV and action potentials that reached at least −10 mV; most overshot 0 mV. We routinely monitored and balanced the bridge during the recordings, and we also measured the input resistance by determining the slope of the linear portion of the *I-V* relationship.

In some experiments for which we had neurobiotin in the recording electrode, we iontophoresed this dye into the cell with depolarizing current steps (200–500 pA in steps of 200–400 ms at 0.5–2 Hz for 1–3 min). This was done at the end of electrophysiological recording. After each such iontophoretic injection, we processed the slice with a standard protocol to reveal the neurobiotin (Zhan and Troy 1997) and assess the morphology of the labeled cell with the light microscope.

### *Model*

Our experimental observations (see RESULTS) demonstrated that threshold behavior and excitability of $Ca^{2+}$ spikes were similar in the presence or absence of TTX (Hernández-Cruz and Pape 1989; Jahnsen and Llinás 1984a,b). Thus we chose for our computations a minimal Hodgkin-Huxley type of model that neglects the primary currents involved in generating and shaping action potentials. Our model includes those currents that we believe capture the essence of our observed activation of $Ca^{2+}$ spikes. Because our main goal for modeling here is qualitative understanding of threshold and latency phenomena under current clamp mode, we sought to obtain semiquantitative agreement, rather than detailed quantitative fits, of simulated results with experimental data.

Exploratory simulations were performed with the computer program Cclamp, developed by Huguenard and McCormick (1994). The basic behaviors of low-threshold excitability were obtained using the "$I_T$" case and "blocking" several voltage-dependent currents until we identified our candidate model. Thus we developed a minimal model for generation of $Ca^{2+}$ spikes that mimics our experimental results.

The current balance equation is

$$C\frac{dV}{dt} = -(I_T + I_A + I_{K-leak} + I_{Na-leak}) + I_{app} \quad (1)$$

where $I_T$ is the "T type" low-threshold $Ca^{2+}$ current, $I_A$ is a transient $K^+$ current, the leakage components ($I_{K\text{-}leak}$ and $I_{Na\text{-}leak}$) are ohmic, and $I_{app}$ represents any current injected into the cell; $V$ is membrane potential (in millivolts); $t$ is time (in milliseconds); and $C$ is total capacitance, equal to 290 pF, corresponding to a cell model with a surface membrane area of 29,000 $\mu m^2$. We used the formulations for $I_T$ and $I_A$ found in the computer program Cclamp of Huguenard and McCormick (1994) and based on their earlier voltage-clamp data (summarized in McCormick and Huguenard 1992). The model uses the Goldman-Hodgkin-Katz formulation for $I_T$ as

$$I_T = P_T m_T^2 h_T \frac{Vz^2F^2}{RT}\left[\frac{Ca_{int} - Ca_{ext}\exp\left(\frac{-zFV}{RT}\right)}{1-\exp\left(\frac{-zFV}{RT}\right)}\right] \quad (2)$$

where $P_T$ is the maximum permeability of an open channel (30 $cm^3$/s), $z = 2$, $Ca_{int}$ and $Ca_{ext}$ are the concentrations of $Ca^{2+}$ inside and outside the cell, respectively (assumed fixed in our model at 50 nM and 2 mM, respectively); F, R, and T are Faraday's constant, the gas constant, and absolute temperature, respectively (Hille 1992). The transient $K^+$ current is given by

$$I_A = g_A m_A^4 h_A (V - V_K) \quad (3)$$

with the reversal potential $V_K = -105$ mV and $g_A = 2$ $\mu$S unless stated otherwise. The leakage currents are given by

$$I_{Na\text{-}leak} = g_{Na\text{-}leak}(V - V_{Na}) \quad (4)$$

and

$$I_{K\text{-}leak} = g_{K\text{-}leak}(V - V_K) \quad (5)$$

where $g_{Na\text{-}leak} = 2.65$ nS, $g_{K\text{-}leak} = 7$ nS, and $V_{Na} = 45$ mV. The general form for the gating dynamics of the voltage-gated channels is

$$\frac{dx}{dt} = \frac{\phi[x_\infty(V) - x]}{\tau_x(V)} \quad (6)$$

where $x = m_T$, $h_T$, $m_A$, or $h_A$ with

$$x_\infty(V) = \frac{1}{1 + \exp\left[\frac{-(V - \theta_x)}{k_x}\right]} \quad (7)$$

The specific parameter values (in millivolts) are $\theta_{m_T} = -60.5$, $k_{m_T} = 6.2$, $\theta_{h_T} = -84$, $k_{h_T} = -4.03$, $\theta_{m_A} = -60$, $k_{m_A} = 8.5$, $\theta_{h_A} = -78$, $k_{h_A} = -6$, and the ''time-constant'' functions are

$$\tau_{m_T} = \frac{1}{\exp\left(\frac{V + 131.6}{-16.7}\right) + \exp\left(\frac{V + 16.8}{18.2}\right)} + 0.612 \quad (8)$$

$$\tau_{h_T} = \exp\left(\frac{V + 467}{66.6}\right) \quad \text{if } V < -80 \text{ mV} \quad (9)$$

$$= \exp\left(\frac{V + 21.88}{-10.2}\right) + 28 \quad \text{if } V \geq -80 \text{ mV} \quad (10)$$

$$\tau_{m_A} = \frac{1}{\exp\left(\frac{V + 35.82}{19.69}\right) + \exp\left(\frac{V + 79.69}{-12.7}\right)} + 0.37 \quad (11)$$

$$\tau_{h_A} = \frac{1}{\exp\left(\frac{V + 46.05}{5}\right) + \exp\left(\frac{V + 238.4}{-37.45}\right)} \quad \text{if } V < -63 \text{ mV} \quad (12)$$

$$= 19 \quad \text{if } V \geq -63\text{mV}$$

We adjusted the gating rates to 33.5°C from Cclamp's set conditions of 23.5°C by using a temperature correction factor, $\theta$, of 3.

All computed results shown here were obtained with the above minimal model using the software XPPAUT (found at http://www.pitt.edu/~phase/). For numerical integration we used the fourth-order, adaptive-step Runge-Kutta method in XPPAUT (with error tolerance, $10^{-5}$). Computations were performed on a Linux/Unix Pentium II workstation.

## RESULTS

### *Experimental observations*

We obtained intracellular recordings in the current clamp mode from a total of 42 neurons from the cat's lateral geniculate nucleus. All appeared to be relay cells on the basis of readily evoked $Ca^{2+}$ spikes. Also we injected with tracer and recovered a subset of five of these cells after the recording session, and their anatomic properties clearly distinguished them as relay cells and not interneurons (Friedlander et al. 1981; Guillery 1966; Sherman and Friedlander 1988). Detailed measurements of resting potential and input resistance were made for a subset of 35 neurons. For these, resting potential was $-60.1 \pm 4.6$ (SD) mV (with a range of $-50$ to $-69$ mV). The input resistances tended to be slightly higher as the cells were hyperpolarized. At rest, the these values were $31.3 \pm 14.7$ MΩ, whereas at 20 mV hyperpolarized to rest, they were $41.5 \pm 16.0$ MΩ; this difference was statistically significant ($P < 0.001$ on a paired *t*-test). Of the 42 cells, 20 were studied extensively before TTX (0.5–1 $\mu$M) was added to the bath to block sodium channels and thus action potential generation; 15 were studied briefly before TTX application and then extensively after; and the remaining 7 cells were studied extensively both before and after TTX application.

Figure 1 illustrates two of the main phenomena we observed for a typical cell from our sample. The cell in Fig. 1*A* was held at the indicated initial membrane potential at which the voltage-dependent $Ca^{2+}$ conductance underlying the low-threshold spike is deinactivated substantially. Figure 1*A*, *top traces*, shows the voltage responses to application of rectangular current injection (indicated *below* the traces) in the presence of TTX, which was applied to show evoked $Ca^{2+}$ spikes without action potentials. With incremental 10-pA steps of current injection, we saw ohmic responses for smaller injections until a voltage threshold was reached, at which point that current injection and all larger ones evoked a $Ca^{2+}$ spike. Interestingly, the amplitude of the $Ca^{2+}$ spike evoked by the smallest suprathreshold current injection was effectively as large as all $Ca^{2+}$ spikes evoked from larger current injections. The input resistance of this cell was ~60 MΩ, and thus each incremental 10-pA current would produce 0.6-mV depolarization. This means that the full-blown $Ca^{2+}$ spike was evoked as a nearly all-or-none event over a range of ≤1 mV in membrane potential (see DISCUSSION for further consideration of this nearly all-or-none behavior). This nearly all-or-none behavior of the $Ca^{2+}$ spike is shown more dramatically in the Fig. 1*A*, *bottom*, in which the evoked $Ca^{2+}$ spikes are overlapped. These overlapped traces also show that the evoked suprathreshold responses exhibit three components: an initial ohmic response (arrow 1), a slow depolarization (arrow 2), and the $Ca^{2+}$ spike itself (arrow 3), although the first two phases are best seen with smaller depolarizing inputs and may be difficult to see with larger ones (see *traces 5* and *6* in Fig. 2*B*). Figure 1, *C* and *D*, shows this same nearly all-or-none behavior for two other geniculate relay cells with TTX application. Figure 1*B* shows that a similar effect was seen in the same cell as shown in Fig. 1*A* before TTX was applied. Fewer traces are illustrated in Fig. 1*B* than in Fig. 1*A* for clarity because the evoked action potentials tend to obscure the key features, but when all incremental 10-pA current injection steps are analyzed, the result is exactly as predicted from Fig. 1*A* with action potentials present.

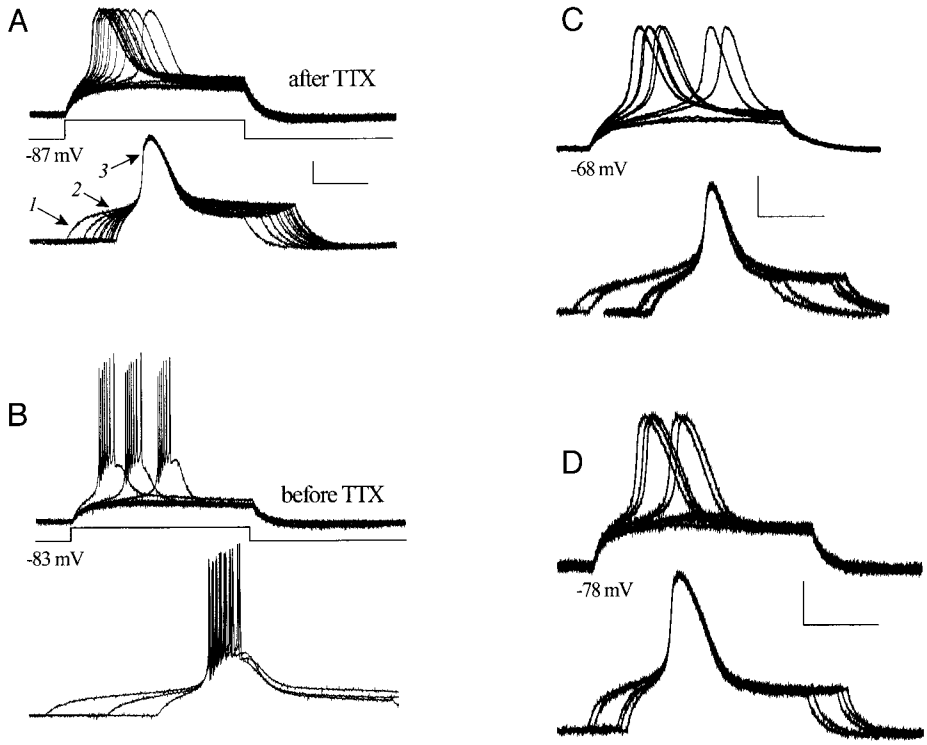


FIG. 1. Activation of low-threshold $Ca^{2+}$ spikes from relay cells in an in vitro slice preparation through the cat's lateral geniculate nucleus. Cells were recorded intracellularly in current-clamp mode. Membrane potentials shown indicate the initial holding potentials. *A*: responses of 1 cell in the presence of 1 $\mu$M TTX. *Top*: original responses. Activation was achieved by injecting depolarizing rectangular current pulses (indicated *below* the traces) starting at 200 pA and incremented in 10-pA steps. Ohmic responses are evoked from smaller currents; the longest latency $Ca^{2+}$ spike evoked is from the smallest suprathreshold current injection, and this latency decreased monotonically as the amplitude of the current injection was increased. *Bottom*: same evoked $Ca^{2+}$ spikes as shown *top* but shifted in time so that they are superimposed. Numbered arrows indicate 3 different phases of the response to the current injections: 1 points to the initial, ohmic response; 2 points to a slower voltage-dependent depolarization; and 3 points to the $Ca^{2+}$ spike. Note that the $Ca^{2+}$ spikes overlap almost perfectly, indicating their nearly all-or-none nature. *B*: same cell as in *A* before application of TTX. *Top*: original recordings; *bottom*: traces adjusted in time to overlap the evoked $Ca^{2+}$ spikes. Latencies of evoked bursts of action potentials decreased with increasing amplitudes of current injection. To avoid extensive overlap in the *bottom traces*, only 3 burst responses are shown. *C* and *D*: 2 further examples with 1 $\mu$M TTX application as in *A*. Although numbered arrows are not shown for these examples, the 3 phases of the evoked response are clearly visible as in *A*. Scale marks represent 100 ms and 10 mV and those in *A* also apply to *B*.

The second main phenomenon we observed is the dramatic decrease in the latency of evoked $Ca^{2+}$ spikes as current injection steps are increased from the first suprathreshold injection. This is seen both in the $Ca^{2+}$ spike latencies (Fig. 1, *A*, *C*, and *D*) and in the latency of action potentials riding the crests of the $Ca^{2+}$ spikes (Fig. 1*B*). In both cases, the latency shift exceeds 150 ms. Interestingly, as can be seen in the overlapped traces of Fig. 1, all $Ca^{2+}$ spikes seem to activate from near the same voltage, as if a simple threshold phenomenon was involved similar to that for an action potential. The slow depolarization leading to the $Ca^{2+}$ spike (indicated by arrow 2 in Fig. 1*A*) has a lower slope for smaller current injections, and this is why it takes longer to reach the threshold to activate the $Ca^{2+}$ spike with smaller current injections. Modeling results described in the following text suggest that this slower depolarization indicated by arrow 2 in Fig. 1*A* is caused by activation of $I_T$ that is too small to be regenerative. The outward ohmic current nearly balances the slowly growing inward $I_T$ during this phase of extended latency. The response becomes regenerative when the threshold is reached to activate the nearly all-or-none $Ca^{2+}$ spike.

NEARLY ALL-OR-NONE NATURE OF $Ca^{2+}$ SPIKES. Figure 2 further illustrates for the same cell as shown in Fig. 1, *A* and *B*, the nearly all-or-none nature of the $Ca^{2+}$ spike during TTX application. Figure 2*A* shows the peak evoked voltage as a function of injected current when the cell initially is held at one of three different initial holding membrane potentials. At a holding potential of $-59$ mV (the resting potential for this cell), there is insufficient deinactivation of the low-threshold $Ca^{2+}$ conductance for activation of $Ca^{2+}$ spikes. The result is that current injection from these holding potentials evokes only an ohmic response, thereby producing a gradual, smooth increase in evoked potential with injected current (Fig. 2*B*, *traces 1–3*). However, at initial holding potentials of $-77$ and $-87$ mV, at which the $Ca^{2+}$ conductance is significantly deinactivated, $Ca^{2+}$ spikes are evoked by suprathreshold depolarizing current injections. Thus we see initial ohmic responses for small current injections until a threshold is reached, at which point a sudden, dramatic increase in evoked membrane voltage is seen (as in Fig. 1). This is because $Ca^{2+}$ spikes are now evoked. After this threshold is reached, larger current injections have little effect on the amplitude of the evoked $Ca^{2+}$ spike (Fig. 2*B*, *traces 4–6*). Note also that the $Ca^{2+}$ spikes evoked from the $-87$-mV holding potential are slightly larger. This is because $I_T$ is more deinactivated when the initial holding potential is $-87$ mV. Also, a larger current step is required from $-87$ mV

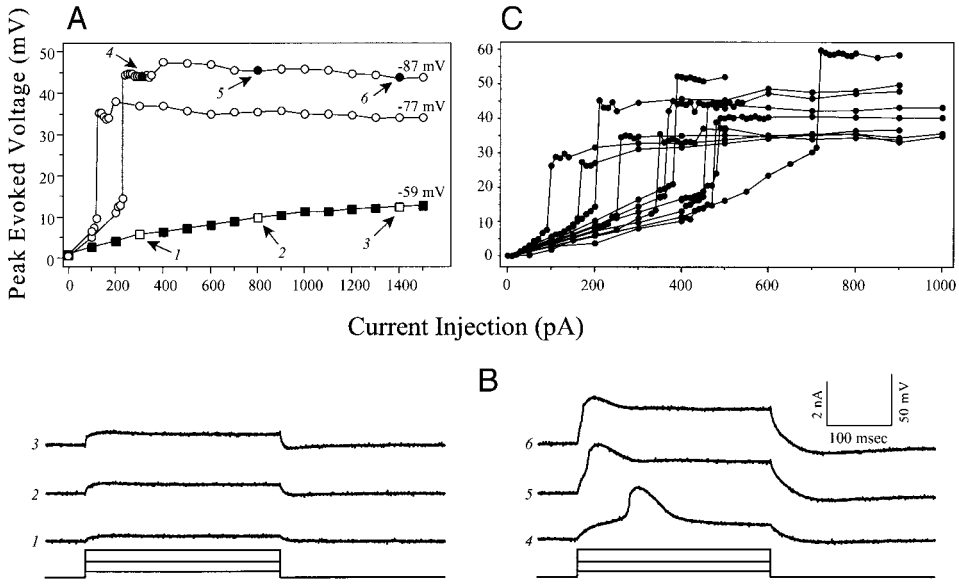


FIG. 2. Relationship between current injection (400-ms pulses) and the evoked responses as in Fig. 1*A* for the same cell in the presence of 1 $\mu$M TTX. *A*: current injection amplitude vs. peak evoked voltage defined as the voltage difference between the peak voltage response and the membrane potential before the current pulse. Shown are 3 curves representing 3 different initial holding potentials as shown. Two of the curves (○ and □) involved holding potentials (−77 and −87 mV) that were sufficiently hyperpolarized that $Ca^{2+}$ spikes were evoked once their activation threshold was crossed. Other curve (● and ■) involved a holding potential at rest (−59 mV) that was too depolarized for generation of $Ca^{2+}$ spikes, and thus mainly ohmic responses were seen. Numbered arrows reflect data points from representative traces in *B*. *B*: representative traces as indicated for generation of the plots in *A*. *C*: current injection vs. amplitude of evoked response for 11 other cells. Initial holding potentials for these cells were −80 to −90 mV, ensuring fairly complete deinactivation of the underlying $Ca^{2+}$ conductance, and injected current was in the form of square wave pulses of 400- to 1,000-ms duration.

to get to the activation threshold for $I_T$ so that this response curve is shifted to the right compared with the curve starting at −77 mV.

The nearly all-or-none activation of the $Ca^{2+}$ spike is fairly typical for our population. From initial holding membrane potentials sufficiently hyperpolarized to deinactivate $I_T$ significantly, every cell of the 22 so studied with TTX application showed a sudden appearance of the $Ca^{2+}$ spike in a single incremental step of current injection, and thus we never activated a significantly smaller $Ca^{2+}$ spike from a just suprathreshold current injection that became much larger as more current was injected. Only when the holding potential was more depolarized, so that $I_T$ was more inactivated, did we see evidence of possibly graded $Ca^{2+}$ spikes (see also VARIATION OF $CA^{2+}$ SPIKE AMPLITUDE WITH DEINACTIVATION LEVEL). Of these 22 cells, 11 were studied with larger incremental current steps of 50 pA before we realized just how sharp the threshold behavior was for activating the full-blown $Ca^{2+}$ spike, so our best examples of this nearly all-or-none behavior came from the 11 cells studied with incremental current steps near threshold of 10 pA. Figure 2*C* summarizes the data as in Fig. 2*A* for these 11 cells. These 11 examples are all taken from initial holding potentials of 20–30 mV below rest, in which there was significant de-inactivation of $I_T$. Every cell in Fig. 2*C* showed a simple ohmic response for smaller current injections interrupted by a sudden rise in voltage to a maximum value over a single 10-pA current step as the $Ca^{2+}$ spikes then were activated. This plot shows the variation in our sample for the amplitudes of $Ca^{2+}$ spikes seen and amount of current injection needed to activate them; variation that is related to, among other properties, differences in input resistance across cells and amount of deinactivation of the low-threshold $Ca^{2+}$ conductance at the initial holding potentials used. Although not shown, we saw the same nearly all-or-none behavior of $Ca^{2+}$ spike activation for all 27 cells studied with no TTX as for the 22 studied with TTX, and often the same cell was studied before and after TTX application.

Figure 3 shows for the same cell the analogous feature as illustrated in Fig. 2 but before TTX application. From four different initial holding potentials, Fig. 3*A* shows the relationship between current injection and the total number of evoked action potentials. In this analysis, the current injection of the abscissa refers to the step from the initial holding membrane potential. In tonic firing mode (initial holding potentials of −47 and −59 mV), there is a gradual, smooth increase in the number of evoked action potentials with increased current injection once threshold is reached (Fig. 3*B, traces 1–3*). However, when the cell is in burst firing mode (initial holding potentials of −77 and −87 mV), a more complicated pattern is seen. With small current injections, action potentials are not evoked until a threshold is reached, at which point six to seven action potentials suddenly appear. This is because the threshold for $Ca^{2+}$ spiking has been reached, and the $Ca^{2+}$ spikes evoke action potentials. The number of evoked action potentials plateaus at six to seven for an extensive range of larger current steps, and then larger current steps begin to increase the number of action potentials gradually. In Fig. 3*B, traces 4* and *5*, which illustrate points on the plateau, show that the evoked response is largely limited to the initial burst of action potentials associated with the $Ca^{2+}$ spike. *Trace 6* from Fig. 3*B*, which is taken from a larger current injection, shows that these large injections activate tonic firing after the initial burst. This is because the long current injection eventually inactivates the low-threshold $Ca^{2+}$ conductance after the initial burst, and if it is then sufficiently large, tonic firing will ensue.

Figure 3*A* plots total number of action potential evoked by

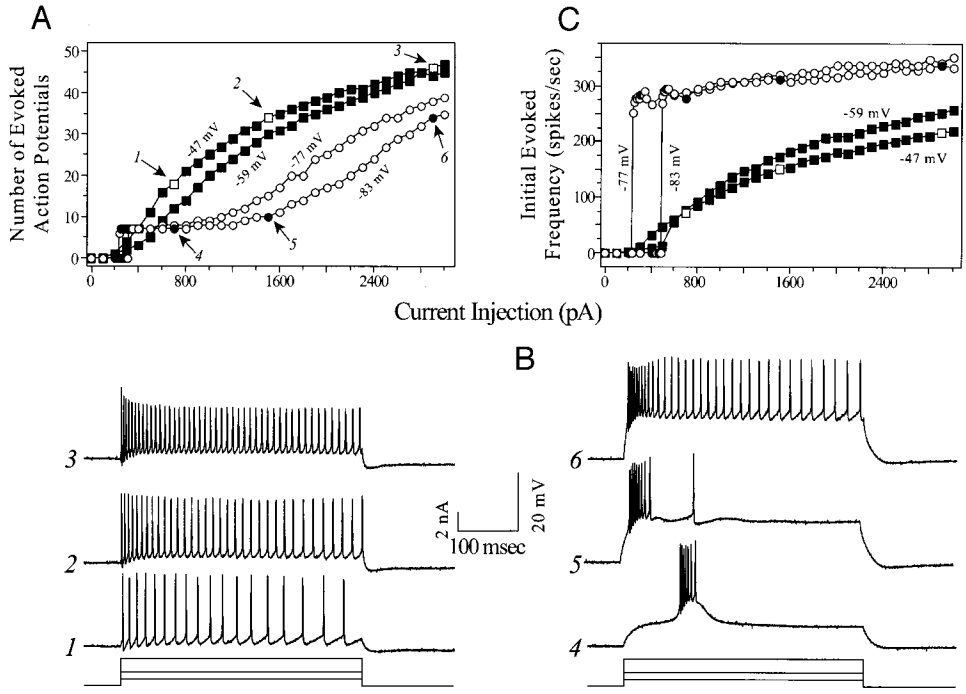


FIG. 3. Relationship between current injection (400-ms pulses) and the evoked action potential responses for same cell as in Fig. 1*B*. *A*: current injection amplitude vs. total number of action potentials evoked. Curves with ○ and □ reflect burst firing, at least initially, whereas the curves with ● and ■ reflect tonic firing. *B*: representative traces for data points indicated in *A*. Note that the small current injection of *trace 4* evokes only a single burst, that the larger injection of *trace 5* evokes an initial burst followed after ~70 ms by a single tonic action potential, and that the even larger injection of *trace 6* evokes an initial burst followed immediately by sustained tonic firing. *C*: current injection amplitude vs. initial firing frequency, which was calculated from the 1st 6 action potentials evoked by the current injection to provide a clearer comparison of burst vs. tonic firing.

the long current injection. However, as just noted, responses evoked from holding potentials of −83 and −77 mV can reflect mixed firing modes, burst followed by tonic for larger current injections. Thus the spike counts indicated in Fig. 3*A* for larger current injections do not accurately reflect the burst/tonic differences. We thus calculated the initial evoked frequency evoked by these current injections by considering the average firing frequency of the initial six action potentials (Fig. 3*C*), and this compares only the initial responses that are purely tonic for the more depolarized holding potentials and purely burst for the more hyperpolarized ones. During tonic firing (initial holding potentials of −47 and −59 mV), the increase in firing frequency is smooth and gradual once threshold is reached. During burst firing (initial holding potentials of −77 and −83 mV), the initial firing frequency shows a sudden step from zero at threshold and increases very gradually thereafter.

The plots of Figs. 2 and 3 represent firing versus the amplitude of the current step injected from the initial holding potential. Figure 4*A* replots the data from Fig. 3*A* with the abscissa adjusted to reflect the total current injected (i.e., initial holding current required for initial holding potential plus the depolarizing step); Fig. 4, *B* and *C*, shows this relationship for two other representative relay cells. Note that at around threshold levels of current injection, burst firing (Fig. 4, ◯) occurs at lower levels of injected current than does tonic firing (■). Thus burst firing occurs at a lower membrane potential, which reflects the ''low-threshold'' nature of the $Ca^{2+}$ spike. Furthermore, although not illustrated here, burst firing commences at a membrane potential that is hyperpolarized with respect to rest (i.e., negative total injected current), whereas tonic firing begins at a membrane potential that is depolarized with respect to rest (i.e., positive total injected current), and this was seen for all other cells studied. Finally, as we have shown earlier, large current injections always produce tonic firing, even if the initial response was in burst mode (see Fig. 3). Thus for the larger current injections that produce tonic firing (>1,200 pA in Fig.

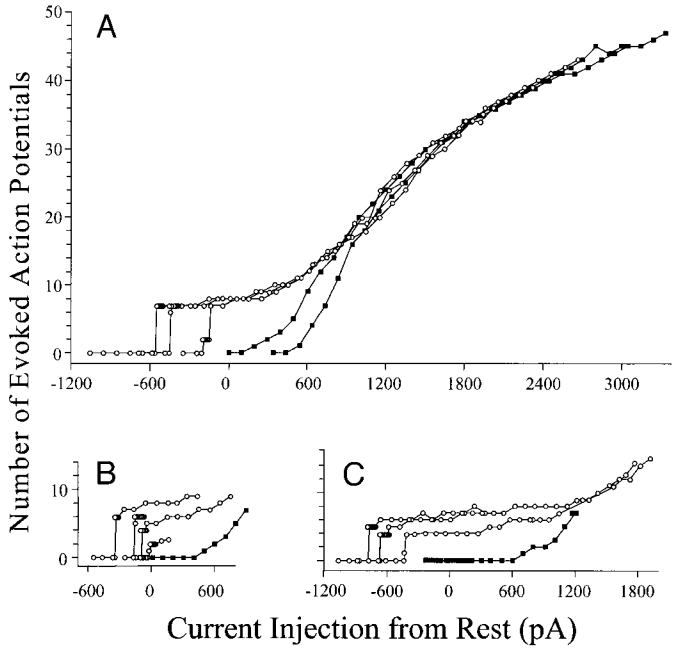


FIG. 4. Comparison between burst and tonic firing evoked by current injections without TTX. Curves with ○ represent burst firing, and those with ■ represent tonic firing. Unlike the plots in Fig. 3 in which the abscissas are the amplitude of the depolarizing pulse from the holding potential, the abscissas in these plots are the total current injected (i.e., the sum of the current used to move the cell from rest to the initial holding potential and the depolarizing current step). *A*: same data as plotted in Fig. 3*A*, except that the abscissa is recalculated to reflect the total current injection. Of particular interest is the range of near-threshold current injections, which show that burst firing always can be evoked with less current injection than is the case for tonic firing. For much larger depolarizing currents, which evoked strong tonic firing even after an initial burst, the curves largely overlap. Note that the activating thresholds for burst firing are hyperpolarized with respect to those for tonic firing. *B* and *C*: data plotted as in *A* for 2 additional cells, showing only the range of near-threshold current injections. Again, bursts are evoked with less current injection than is the case for tonic firing.

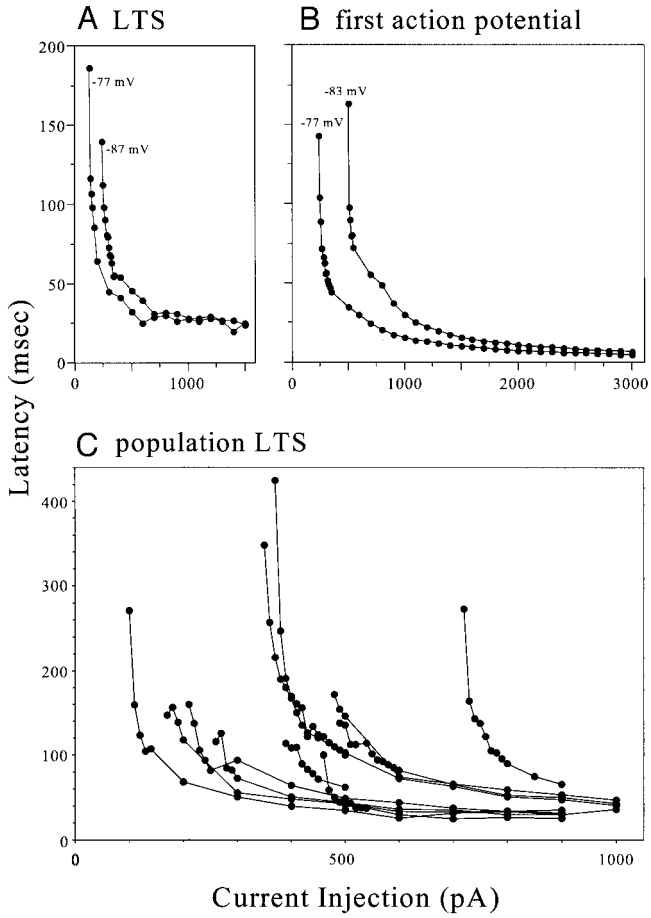


FIG. 5. Relationship between current injection and response latency. *A*: effect of current injection on response latency during 1 $\mu$M TTX application for same cell as shown in Fig. 1*A*. Latency is measured from the initiation of the depolarizing pulse to the peak of the evoked low-threshold $Ca^{2+}$ spike (LTS). Relationships are shown for the 2 initial holding potentials shown. *B*: relationships for the same cell as in *A* before TTX application for the 2 initial holding potentials shown before TTX application. Latency was measured from the start of the current injection to the peak of 1st action potential of the evoked burst. *C*: effect of current injection on response latency of $Ca^{2+}$ spike for population of additional 11 cells in the presence of 1 $\mu$M TTX.

4*A*), the firing rates are roughly the same regardless of the all initial holding potentials.

LATENCY OF LOW-THRESHOLD $Ca^{2+}$ ACTIVATION. The latency of the evoked $Ca^{2+}$ spike becomes considerably shorter with greater current injection (see Fig. 1). This appears to be related to the rate of rise of the initial depolarizing response before a near-threshold voltage is reached to initiate the $Ca^{2+}$ spikes. Figure 5, *A* and *B*, plots the relationship between current injection and these latencies for the same cell as shown in Fig. 1, *A* and *B*. From both initial holding potentials ($-77$ and $-87$ mV) during TTX application, the latency of $Ca^{2+}$ spike was reduced gradually as the current injections increased, from 186 to 25 ms at a holding potential of $-77$ mV and from 139 to 24 ms at a holding potential of $-87$ mV (Fig. 5*A*). A similar effect is seen before TTX application when the latency to the first action potential peak riding the crest of a $Ca^{2+}$ spike is plotted against injected current (Fig. 5*B*). These latencies were reduced from 143 to 4 ms at a holding potential of $-77$ mV and from 164 to 7 ms at a holding potential of $-83$ mV. The latency reduction was sharp for initial suprathreshold current injections and became more gradual with larger current injections.

Figure 5*C* shows that the pattern of latency versus injected current for the same 11 cells illustrated in Fig. 2*C*. The maximal latencies we observed to activation of $Ca^{2+}$ spikes with just suprathreshold current injections in the presence of TTX was 235 $\pm$ 80 ms with a range of 139–425 ms. The activation currents had to be ~200–400 pA suprathreshold before the latency reduction became asymptotic. Although not illustrated, the 27 cells studied without TTX showed the identical pattern, meaning that the latency of the first spike evoked during burst firing decreased as current injections increased from threshold to elicit the $Ca^{2+}$ spike.

The data plotted in Fig. 5 reflect activation from long current pulses of 200–1,000 ms, raising the possibility that long-latency $Ca^{2+}$ spikes require long current pulses. We used very brief current pulses (5 ms) to test this on a subset of seven cells, and an example is shown in Fig. 6. Not only are brief injections of this sort, which temporally are similar to EPSPs, sufficient to activate $Ca^{2+}$ spikes, but as with the longer pulses these activate $Ca^{2+}$ spikes with a latency that decreases with increasing amplitude of the injected current. Also, the $Ca^{2+}$ spikes are evoked long after the termination of the current pulses.

VARIATION OF $Ca^{2+}$ SPIKE AMPLITUDE WITH DEINACTIVATION LEVEL. The preceding results show that the $Ca^{2+}$ spike is activated effectively in a nearly all-or-none manner. Thus with 10-pA current injection steps, a depolarizing input activates only an ohmic response if subthreshold and a full-blown $Ca^{2+}$ if suprathreshold. We cannot rule out the possibility that partial $Ca^{2+}$ spikes might have been seen if we used smaller injection increments, but the fact that we never saw this in any of our cells suggests that the incremental range of current injections over which partial $Ca^{2+}$ spikes might be activated is much less than 10 pA and thus $\leq$1 mV of depolarization for a cell with an input resistance of 50 M$\Omega$. In theory (see DISCUSSION), graded responses may be expected, although probably with quite a steep dependence on stimulus amplitude, which is qualitatively what we have seen experimentally.

This implies that the proportion of T channels deinactivated by any particular initial holding potential limits the maximal amplitude of the $Ca^{2+}$ spike realizable from that holding state. Furthermore as long as this proportion is above a certain value

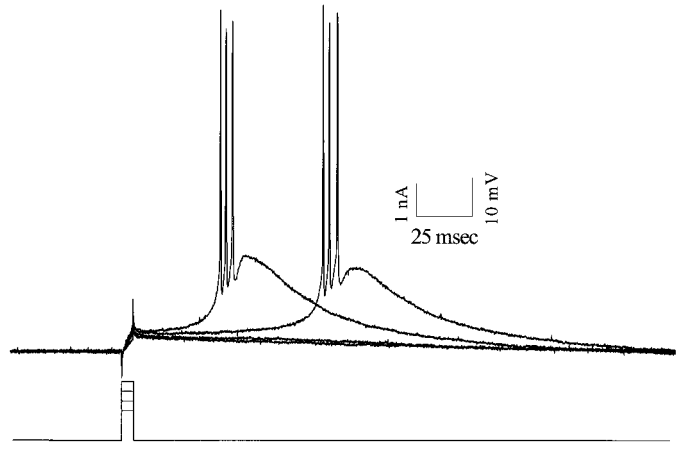


FIG. 6. Activation of $Ca^{2+}$ spikes with brief depolarizing pulses (5-ms duration). Shown are 4 superimposed traces, including responses to the largest 2 subthreshold injections and to the smallest 2 suprathreshold injections. No TTX was present for these responses. $Ca^{2+}$ spikes were evoked well after the cessation of the current injection, and the latency of the evoked $Ca^{2+}$ spikes dropped dramatically as the suprathreshold injection was increased in amplitude.

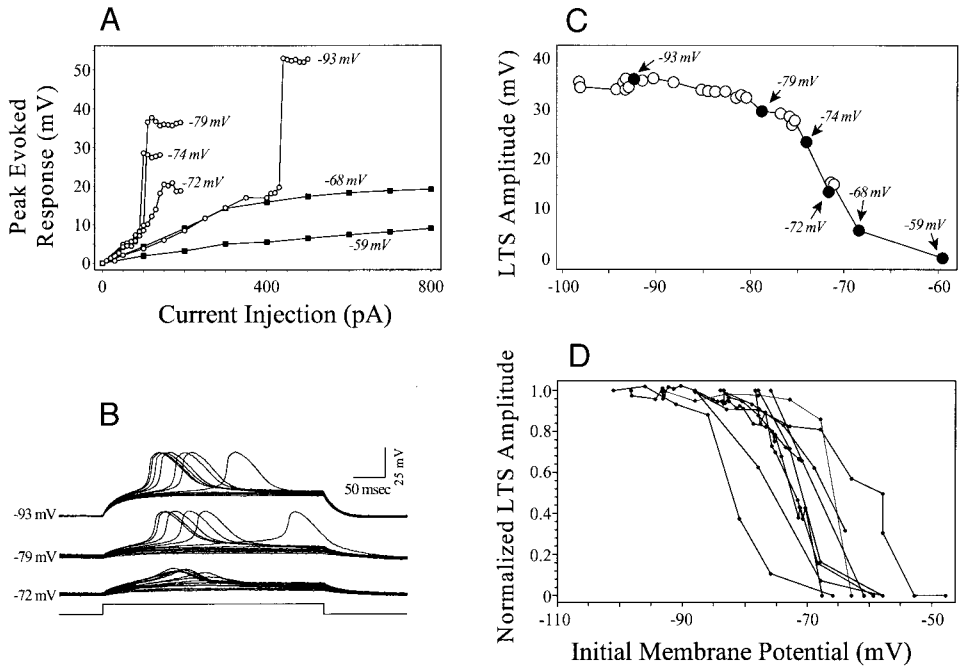


FIG. 7. Effect of deinactivation on $Ca^{2+}$ spike amplitude. *A*: relationship between current injection and peak evoked response in presence of 1 $\mu$M TTX as in Fig. 2. Different initial holding membrane potentials are shown and were achieved with constant hyperpolarizing currents. Series of depolarizing current pulses incremented by 10 pA and with a duration of 300 ms was injected to evoke ohmic responses (subthreshold currents) or $Ca^{2+}$ spikes (suprathreshold currents). Curves with ○ represent activation of $Ca^{2+}$ spikes, and those with ■ indicate only ohmic responses. *B*: representative series of traces from the data plotted in *A* for activation of $Ca^{2+}$ spikes from different initial holding membrane potentials. Note that for the relatively depolarized initial holding potential (−72 mV), graded amplitudes of response are seen that may or may not involve $Ca^{2+}$ spikes (see text for details). *C*: relationship between the initial holding membrane potential and the maximum $Ca^{2+}$ spike amplitude for same cell as is illustrated in Fig. 1*A*. Ordinate represents the amplitude of the $Ca^{2+}$ spike evoked from just suprathreshold current injections. LTS amplitude is defined here as the voltage difference between the peak of the $Ca^{2+}$ spike and the level of the ohmic response remaining ≥100 ms after the $Ca^{2+}$ spike ended. ●, 6 initial membrane potentials from which the plots in *A* are taken. *D*: relationship between initial holding membrane potential and normalized amplitude of evoked $Ca^{2+}$ spike for 11 other relay cells.

(see following text), it is more than enough to ensure that a nearly all-or-none $Ca^{2+}$ spike is evoked virtually independent of the amplitude of a suprathreshold depolarizing current injection. This predicts that the more hyperpolarized the holding potential, the more that deinactivation will occur, and the larger the $Ca^{2+}$ spike that will be activated. Figure 2*A* shows some evidence for this because the amplitudes of the $Ca^{2+}$ spikes activated from −87 mV are larger than those activated from −77 mV.

This is explored more systematically for the same cell in Fig. 7, *A–C*, studied after TTX application. In this experiment, current steps were injected into the cell from a wide range of initial holding potentials. When the initial holding potential is hyperpolarized enough to permit substantial deinactivation of $I_T$ (i.e., −93, −79, and −74 mV), the $Ca^{2+}$ spike is activated in a nearly all-or-none manner (Fig. 7, *A* and *B*). At a slightly more depolarized initial holding level (i.e., −72 mV), the evoked response appears to be graded very slightly. However, the response is very small, and it is difficult to determine whether it represents the slow depolarizing phase (arrow 2 in Fig. 1*A*), the all-or-none $Ca^{2+}$ spike (arrow 3 in Fig. 1*A*), or both. When the initial membrane holding potential is more depolarized (−59 mV, which is near rest, and −68 mV), no discernable $I_T$ is evoked and a purely ohmic response occurs. Figure 7*C* plots the different holding potentials versus maximum $Ca^{2+}$ spike amplitude, which is the first suprathreshold response except for occasional graded responses evoked from more depolarized holding potentials (see Fig. 7*B*, *bottom*). Thus while depolarizing inputs to these cells activate $Ca^{2+}$ spikes in a nearly all-or-none fashion, their amplitude can be controlled effectively by the level of deinactivation, which in turn is determined by the level and duration of hyperpolarization preceding the activating input. Also, very slightly graded $Ca^{2+}$ spike amplitudes may be seen for a narrow range of holding potentials at which $I_T$ is deinactivated less thoroughly (e.g., the −72-mV holding potential example in Fig. 7, *A* and *B*), although even here it is not clear if this response is a full-blown $Ca^{2+}$ spike (see preceding text). Figure 7*D* shows the same relationship as in Fig. 7*C* for a sample of 10 relay cells.

### *Theoretical observations*

Our minimal model with only two voltage-dependent currents, $I_T$ and $I_A$, shows the basic features of generation of $Ca^{2+}$ spikes as seen experimentally (Fig. 8; compare with Figs. 1 and 7). These features include a nearly constant amplitude of the evoked $Ca^{2+}$ spike for different current steps from a given holding level, a dramatic effect on latency of the evoked $Ca^{2+}$ spikes over a narrow range of suprathreshold current injection amplitudes, increasing gradation and decreasing amplitude of the $Ca^{2+}$ spike with less hyperpolarized holding levels. A response for a suprathreshold stimulus shows an early small depolarization (the initial ohmic response, see arrow 1 in Fig. 1*A*), followed by a phase of slow depolarization (see arrow 2 in Fig. 1*A*), and finally the $Ca^{2+}$ spike (see arrow 3 in Fig. 1*A*).

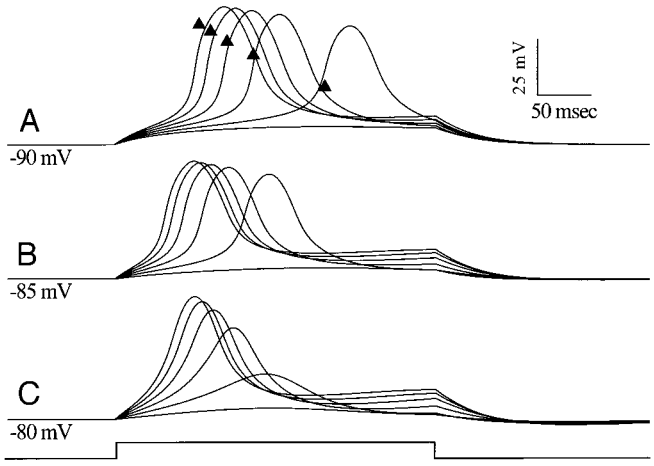


FIG. 8. Simulated membrane potential time courses showing responses to depolarizing current steps for minimal model of relay cell without action potential currents but with the $K^+$ ''leak'' conductance and $I_A$ present. Three different initial holding membrane potentials are shown. *Below* the voltage traces is shown the time course of the 400-ms current injection. In all cases, as in the experimental data, the minimum suprathreshold current injection evoked the $Ca^{2+}$ spike with the longest latency, and this latency reduced to asymptotic levels as the amplitude of current injections increased (see Figs. 1, 2, 8, and 9). Current injections are given as $I_p = I_{p,\,o} + j*\Delta I_p; j = 1,2$. *A*: initial holding potential of −90 mV, corresponding to holding current of −258 pA with $I_{p,\,o}$ = 48 pA and $\Delta I_p$ = 10 pA. ▲, relative peak values of $I_T$ (using the holding membrane potential as a reference line) and their times of occurrence. *B*: initial holding potential of −85 mV, corresponding to holding current of −220 pA with $I_{p,\,o}$ = 20 pA and $\Delta I_p$ = 16.7 pA. *C*: initial holding potential of −80 mV, corresponding to holding current of −188 pA with $I_{p,\,o}$ = 10 pA and $\Delta I_p$ = 12 pA. Response amplitude diminishes as holding potential increases to less negative levels (*A–C*), as in experimental data from Figs. 11 and 12. Range of latencies is largest and gradation of response amplitude is smallest for the most negative holding potential (*A*).

To evoke a $Ca^{2+}$ spike from the model, as in the experimental data, the initial holding membrane potential must be hyperpolarized adequately so that $I_T$ has been deinactivated sufficiently. Under these conditions, the peak amplitude of the $Ca^{2+}$ spike is nearly independent of the amplitude of the suprathreshold current step. When the simulation starts with more $I_T$ deinactivation (Fig. 8, *A* and *B*), the $Ca^{2+}$ spike appears in a nearly all-or-none fashion. If the holding potential is less hyperpolarized, meaning more of the $I_T$ is inactivated, responsiveness may become more graded (Fig. 8*C*). The behavior is thus not strictly all or none, as becomes apparent when the level of $I_T$ inactivation is relatively high, and this correlates with the experimental observation that graded responses can be obtained from relatively depolarized holding potentials (see *trace 3* of Fig. 10; see also DISCUSSION).

DISSECTING THE MODEL'S $Ca^{2+}$ SPIKE. To understand the effect of just suprathreshold activating currents on the latency of $Ca^{2+}$ spikes, we have dissected in Fig. 9 the time course of the response in Fig. 8*A* to the minimum suprathreshold current injection, which evoked the longest-latency $Ca^{2+}$ spike. Also shown is the time course of $h_T$ (- - -), which is the fraction of channels not inactivated: the larger is $h_T$, the more $I_T$ is deinactivated, and as expected depolarization during the $Ca^{2+}$ spike causes $h_T$ to drop with a time scale of tens of milliseconds. Figure 9*B* shows the interplay between the different currents during this response. The early depolarization originates from the combination of injected current and leakage current ($I_{leak} - I_{app}$; — - —), which is initially inward. This current approaches zero at around −83 mV, and the membrane would come to rest there if no other currents were involved. However, $I_T$ (— — —), beginning from near zero at the (deactivated) holding state, continues to grow slowly. Although the leakage and injected current combination becomes outward, this is more than offset by the slowly growing $I_T$, which is inward. Until relatively late in the response, these components remain small and nearly cancel each other. Thus while the net current (—) is depolarizing during period of slow depolarization before initiation of the $Ca^{2+}$ spike, its time course is not monotonic. It jumps up, then decreases to a minimum, becoming quite small and thereby stalling the depolarization. $I_T$ and membrane voltage continue to grow slowly together until the membrane voltage enters the regime for regenerative activation of $I_T$. The nonlinear voltage dependent gating of $I_T$ determines the voltage range in which the sharply rising upstroke of the $Ca^{2+}$ spike occurs.

Several additional features in Fig. 9 are noteworthy. First, during a long-latency activation of a $Ca^{2+}$ spike, a considerable degree of inactivation of $I_T$ may occur before the $Ca^{2+}$ spike is initiated (see $h_T$ in Fig. 9*A*). Because the time constant of $h_T$ is voltage dependent and large in the −100- to −70-mV range, less inactivation occurs with shorter latencies for initiation of the $Ca^{2+}$ spike. Second, the level of $I_A$ is insignificant throughout all of the response before activation of the $Ca^{2+}$ spike and therefore plays only a minor role in determining the latency of the $Ca^{2+}$ spike. Third, the reduction in $h_T$ before activation of the $Ca^{2+}$ spike suggests that a smaller $I_T$ is generated when the

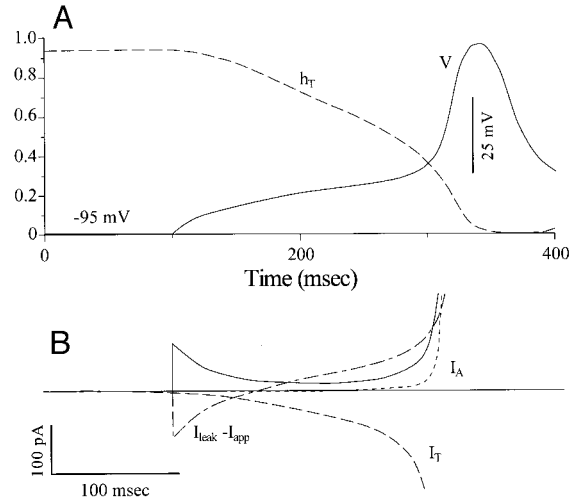


FIG. 9. Time courses of variables and individual ionic currents during a simulated response of a $Ca^{2+}$ spike as in Fig. 8. Response shown is to a just-suprathreshold current injection (97 pA), so the $Ca^{2+}$ spike has a long latency. Initial holding membrane potential is −95 mV achieved with a holding current of −300 pA. *A*: time courses of membrane voltage (*V*, —) and inactivation variable ($h_T$, - - -) to a depolarizing current pulse starting at 100 ms. Ordinate reflects relative values for *V* and $h_T$. Membrane potential initially relaxes with a membrane time constant (of ~30 ms) to a more slowly rising phase before the $Ca^{2+}$ spike begins abruptly. Some inactivation of $I_T$ occurs ($h_T$ decreases) during the initial depolarization before the initiation of the $Ca^{2+}$ spike, and the inactivation then proceeds rapidly during the upstroke of the $Ca^{2+}$ spike. *B*: membrane currents during response shown in *A;* inward currents are plotted down. $I_T$ (— — —) grows slowly and then very fast to initiate the $Ca^{2+}$ spike. $I_A$ (- - -) makes little contribution until the $Ca^{2+}$ spike begins. Combined stimulating and leakage currents ($I_{app}$ and $I_{leak}$, respectively; — - —) is initially inward then becomes outward, opposing $I_T$. Sum of currents with negative sign (—) is proportional to d*V*/d*t*, and it thus has a local flat minimum during period before the $Ca^{2+}$ spike is initiated. Horizontal — corresponds to 0 current.

latency is longer (i.e., from just suprathreshold current injections). The triangular data points in Fig. 8*A* indicate the relative peak values of $I_T$ (and times of occurrence) for the spikes, showing the decrease with longer latency. Nevertheless, the case in Fig. 9*A* illustrates that a sizable $Ca^{2+}$ spike proceeds even if $h_T$ drops below the 50% level. Finally, in passing, we note that $I_T$ peaks and is inactivated almost completely before the peak of the $Ca^{2+}$ spike occurs.

Although $I_A$ is not the determining factor for the latency of evoked $Ca^{2+}$ spikes in our model, it does control the amplitude of these spikes. It is the only nonlinear, voltage-dependent, outward current in this minimal model. In thalamic relay cells, other $K^+$ currents also contribute to limiting the $Ca^{2+}$ spike amplitude (Huguenard and McCormick 1992). Correspondingly, we have used the model to show that other $K^+$ currents acting alone also could restrict the $Ca^{2+}$ spike amplitude (not shown). However, other active $K^+$ currents, without $I_A$ present, affect the low-threshold spike rising phase differently. With $I_A$, the rise is less rapid and the depolarization peak is rounded. Without $I_A$, the other $K^+$ currents limit amplitude abruptly by interrupting a very rapid upstroke, leaving a cornered leading edge, sometimes with a tiny overshoot (not shown). The other $K^+$ currents that we considered have higher thresholds (like the delayed rectifier) or are activated by $Ca^{2+}$ and so must follow after the recruitment of $I_T$. They only can play a role after the upstroke of the $Ca^{2+}$ spike is well underway, unlike $I_A$, which begins acting in the subthreshold regime. These other candidates do not influence the latency effects that we have seen.

We have focused here on $I_A$ for amplitude control because of the above observations and because we wanted to explore its effect on response latency, an often-implicated role for $I_A$ (McCormick 1991; Rogawski 1985; Storm 1988). From Fig. 9*B*, where $I_A$ affects latency to peak only slightly, we predict, and Fig. 10*A* confirms, that similar long latencies and threshold behaviors occur when $I_A$ is blocked. Furthermore, Fig. 10*B* shows that changing the effectiveness of $I_A$ by changing its inactivation time constant has virtually no effect on the latencies of $Ca^{2+}$ spikes. $I_A$, however, does affect the amplitude of the $Ca^{2+}$ spikes because no $I_A$ permits the largest $Ca^{2+}$ spikes (Fig. 10*A*), and increasing the inactivation time for $I_A$ reduces the amplitude of these $Ca^{2+}$ spikes (Fig. 10*B*). In any case, we conclude that the properties of $I_T$ alone can account for the observed latency effect.

The simulation in Fig. 10*A* of a pure $Ca^{2+}$ spike, with $I_T$ and leakage as the only intrinsic currents, enables us to examine further the threshold properties of activating a full-blown $Ca^{2+}$ spike. Here we see that the $Ca^{2+}$ spike has a characteristic take-off from a critical voltage range, and this may be considered a quasithreshold like that of the action potential (see also Fig. 1). Another way to see this is with phase plane plots that show the response trajectory projected onto a plane of two dynamic variables. Figure 11*A* shows the responses from Fig. 10*A* plotted as curves of $C*dV/dt$, where $C$ is membrane capacitance and $C*dV/dt$ is ionic plus injected current versus voltage ($V$). Because $t$ is the parameter along a trajectory, the need to translate curves in time to compare transient responses (as done in Fig. 1) is obviated. Flow along the trajectories is clockwise (arrows in Fig. 11*A*), starting at the holding state to the far left. During the period before the $Ca^{2+}$ spike is evoked, the trajectory is flat and lies just above the zero current axis. The triangular portion of the curves represent the upstrokes of the $Ca^{2+}$ spikes, and the upper apex coincides with the maximum rate of rise. The peaks of the $Ca^{2+}$ spikes occur where the trajectory crosses the zero-current axis, at the right corner. The recovery phase of the low-threshold $Ca^{2+}$ conductance corresponds to when the trajectory lies below the zero-current axis. The fact that these several trajectories for different stimuli nearly superimpose during their early rising phases (lower left side of the triangles) shows the common mechanism of activation of a full-blown $Ca^{2+}$ spike within in a critical and limited voltage range, producing the appearance of a quasithreshold for membrane voltage. The underlying mechanism, which is a fast, voltage-gated amplification of $I_T$, also may be visualized from these phase planes. Figure 11*B* shows a selected example of a $Ca^{2+}$ spike evoked with a long latency, redrawn from Fig. 11*A*, together with the component currents. The overall membrane potential is represented by the solid curve, and the open circles along it represent equally spaced, 5-ms increments to illustrate motion along the trajectory (i.e., faster where the ○ are farther apart). Here, one sees that the upstroke portion of the $Ca^{2+}$ spike, especially the early phase, is accounted for by the dynamics of $I_T$, which is shown by the curve with short dashes. This trajectory explicitly shows us the nonlinear relationship of $I_T$ to voltage during a $Ca^{2+}$ spike. Regenerative growth of $I_T$ drives the acceleration in voltage, where $dV/dt$ is increasing. Although this triangular portion is reminiscent of the instantaneous current-voltage ($I$-$V$) relation for $I_T$ (with inactivation, $h_T$, held fixed) the two are not identical because here $h_T$ is changing with time. In contrast to the nonlinear behavior of $I_T$, the remaining current is linear with respect to voltage, as seen by the lower curve (— - —) in Fig. 11*B*.

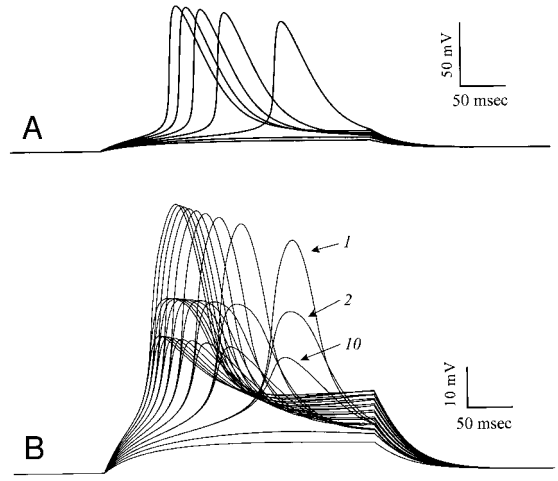


FIG. 10. Simulated membrane potential time courses showing responses to depolarizing current steps as in Fig. 8 showing effects of $I_A$. Initial membrane potential is −91.7 mV, which is achieved with a holding current of −272 pA. *A*: simulations with all voltage-dependent $K^+$ currents suppressed, including $I_A$. As in the experimental data shown in Fig. 1, the responses to subthreshold current steps are ohmic and to suprathreshold steps are $Ca^{2+}$ spikes. Increasing the suprathreshold current injections significantly reduces the latency of the evoked $Ca^{2+}$ spike with little effect on its amplitude. *B*: simulations similar to *A*, except that $I_A$ is present with a varying inactivation time constant (see *Eq. 11*). Numbered arrows indicate simulations with the normal time constant (1), twice the time constant (2), and 10 times the time constant (10). These changes in $I_A$ affect the amplitude but not the latency of the evoked $Ca^{2+}$ spikes. Thus the latency effect in this model does not depend on $I_A$.

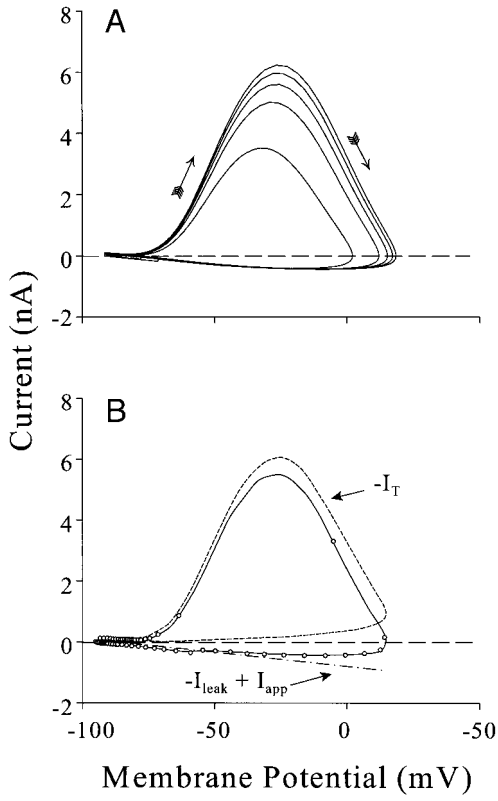


FIG. 11. Trajectories of $Ca^{2+}$ spikes in the voltage-current phase plane. Shown are responses of a reduced model having $I_T$ and $I_{leak}$ but without $I_A$ to various current injection steps from an initial holding membrane potential of −91.5 mV. *A*: series of curves of membrane voltage vs. membrane current, the latter calculated from $C*dV/dt$, where $C$ is capacitance, each curve has a clockwise motion (arrows) with time as a parameter. Initial holding state is at the *far left*. *B*: single curve (—) redrawn from *A*. Shown for comparison are the current-voltage trajectories of the individual components of the total current, which are $I_T$ (- - ) and $I_{leak} - I_{app}$ (— - —); these currents are plotted with reversed sign. At each voltage, the sum of components equals $C*dV/dt$. Note that the rapid phase of the upstroke is nearly equal to the regenerative $I_T$. ○, equal time increments (5 ms) along the trajectory of the $Ca^{2+}$ spike; their wide spacing during the upstroke indicates that it is very rapid.

## DISCUSSION

We have systematically examined certain features of activation of the $Ca^{2+}$ spike in geniculate relay cells, using a combination of current-clamp recording with an in vitro slice preparation and computational modeling. Much of the previous quantitative experimental work directed at the $Ca^{2+}$ spike and the underlying $I_T$ has been done in vitro with voltage-clamp recording, often in acutely dissociated cells (Coulter et al. 1989; Hernández-Cruz and Pape 1989). This body of work has enabled the development of theoretical models for $Ca^{2+}$ spike generation. The models have been shown to mimic some general aspects of $Ca^{2+}$ spike excitability, but there is only a limited set of experimental observations from current-clamp recording that is available for more thorough comparisons. Our primary goal was to provide a more systematic quantitative characterization of threshold, amplitude, and latency properties for $Ca^{2+}$ spike activation in relay cells. We also sought to test if our experimental observations from current-clamp recording are consistent with the voltage-clamp data by using a minimal computational model to simulate current-clamp results from voltage-clamp data. Furthermore we use the model to gain insight into the threshold behavior of $Ca^{2+}$ spike generation.

Our main observations with this approach are fivefold. *1*) The $Ca^{2+}$ spike, when triggered, is nearly all or none, and it in turn evokes a number of action potentials that ride its crest. *2*) The process of activating $I_T$ consists of a slowly depolarizing phase that, if sufficiently strong, activates a later, very fast, depolarization, which is the $Ca^{2+}$ spike. *3*) The initial slow phase of $I_T$ activation has a variable slope that is determined at least partly by the amplitude of initial depolarization, and this, in turn, determines the latency of the nearly all-or-none $Ca^{2+}$ spike. *4*) Although the size of the depolarizing input affects the latency of the evoked $Ca^{2+}$ spike, it has little effect on its amplitude, the spike is evoked in a nearly all-or-none manner. Instead, the amplitude of the $Ca^{2+}$ spike is controlled in current-clamp recording by the extent of membrane hyperpolarization from which the $Ca^{2+}$ spike is evoked. This hyperpolarization affects the degree of deinactivation of $I_T$ and thus the availability of $I_T$ for activation of the $Ca^{2+}$ spike. *5*) Finally, the main observations we have made in our electrophysiological recordings can be simulated from our computational model cell, and the modeling suggests explanations for some of the phenomena we have observed for activation of $Ca^{2+}$ spikes.

### *Amplitude of the $Ca^{2+}$ spike*

Voltage-clamp studies of $I_T$ show that the activation range is fairly extensive, meaning that the underlying conductance grows in a sigmoid fashion over a voltage range of 10–15 mV (Coulter et al. 1989; Crunelli et al. 1989; Hernández-Cruz and Pape 1989). In the model, $k_{mT}$ equals 7.4 mV. Furthermore the activation time constant is based on voltage-clamp measurements at room temperature, whereas our experiments were carried out much closer to body temperature, and warmer conditions increase the rate of activation. In any case, activation of $I_T$ causes rapid depolarization if the membrane voltage is not clamped. Thus in normal conditions (i.e., no voltage clamp), a small depolarizing input may evoke a small initial $I_T$, which will cause further depolarization that increases the $I_T$ in a positive feedback process. Our data indicate that this regenerative process, which is analogous to an autocatalytic chemical reaction (see also Coulter et al. 1989; Crunelli et al. 1989), underlies the generation of $Ca^{2+}$ spikes because they seem to be activated in a nearly all-or-none manner (see Figs. 1–3 and 8, *A* and *B*). This means that, when the cell is in burst mode, it responds to suprathreshold depolarizing inputs with $Ca^{2+}$ spikes that vary little in amplitude or shape, although as noted below, their latency can be quite variable. These features of amplitude, sharpness of threshold, and latency for $Ca^{2+}$ spike activation are not readily evident from the gating properties generated from voltage-clamp studies, but when these data are used to model $I_T$ activation in current-clamp recording, nearly all-or-none behavior is seen. Our current-clamp experiments coupled with the modeling help to further synthesize these voltage-clamp data into understanding $Ca^{2+}$ spike excitability in relay cells, and this also complements previous current-clamp studies.

Although the size of an activating input has little effect on the amplitude of the evoked $Ca^{2+}$ spike, the level of preceding hyperpolarization certainly does. This hyperpolarization level determines the magnitude of $I_T$ deinactivation available at the time when a stimulus is delivered, thereby influencing significantly the amplitude of the $Ca^{2+}$ spike if the input is supra-

threshold. We conclude from these observations that the amount of deinactivation rather than the activating input controls the amplitude of the $Ca^{2+}$ spike. Interestingly, in the model, the amount of $I_T$ recruited depends not only on the extent of hyperpolarization before $I_T$ activation but also on the depolarizing input (see Figs. 8*A* and 11*A*). Because $I_T$ inactivates somewhat during the slow depolarization phase, the extent of this inactivation is greater for longer latencies of $Ca^{2+}$ spike activation. Even though the peak of the conductance associated with $I_T$ may drop substantially with increasing latency, the computed voltage peak of the $Ca^{2+}$ spike is diminished only slightly (see further for discussion). This is because the relationship between conductance and voltage response is nonlinear and sublinear for large conductance inputs, so that, for example, halving the conductance does not half the peak voltage.

The amplitude of the $Ca^{2+}$ spike is also limited by active $K^+$ currents. We have not explored the effects of these other currents in detail, although we expect that, for our experiments with TTX, the high-threshold currents like the delayed rectifier are far less activated than they might otherwise be. Our modeling results suggest that $I_A$, which also operates in the low-voltage regime where $I_T$ is activated, contributes significantly to limiting the amplitude of the $Ca^{2+}$ spike. Further study on the properties and spatial localizations of $I_A$ and other $K^+$ conductances is merited to characterize more fully their role in burst mode firing in relay cells.

There is now ample data from lightly anesthetized and awake animals that thalamic relay cells firing in burst mode effectively transmit peripheral information to cortex (Guido and Weyand 1995; Sherman 1996). These nearly all-or-none amplitude properties of the $Ca^{2+}$ spike thus have important implications for how information is relayed through the lateral geniculate nucleus and, presumably, through other thalamic nuclei as well. Suppose that the amplitude of the $Ca^{2+}$ spike is monotonically related to the number of action potentials in the evoked burst. This implies that a relay cell in burst mode will respond to suprathreshold EPSPs with little relationship between the amplitude of the EPSP and the number of action potentials in the burst. For a given level of hyperpolarization preceding the EPSP and thus a given level of $I_T$ deinactivation, essentially all suprathreshold EPSPs will evoke the same amplitude of response. Even if the deinactivation level of the $I_T$ varies during burst firing because of fluctuations in membrane potential, the nearly all-or-none nature of the evoked $Ca^{2+}$ spike means that no clear relationship will be present between the input EPSP amplitude and the evoked response. When the same relay cell responds in tonic mode, larger suprathreshold EPSPs will evoke more action potentials (see Fig. 4*A*). However, within a narrow range of initial membrane potentials for which $I_T$ is less deinactivated, the evoked response, which may or may not involve a $Ca^{2+}$ spike, may be very slightly graded (Fig. 7) and related in amplitude to the amplitude of the EPSP. Unless burst firing was somehow limited to this small range of initial membrane potentials and reduced levels of $I_T$ deinactivation, which seems unlikely but must be empirically tested in behaving animals, burst firing would reflect poorly the stimulus amplitude.

In the visual system, we can imagine how this would relate to the response of geniculate relay cells to varying contrasts because larger contrasts evoke stronger responses in retinal inputs to these relay cells (e.g., Troy and Enroth-Cugell 1993), and this, in turn, leads to larger EPSPs. With the cell in burst mode, it would be unable to encode these varying contrasts in its response to cortex, because all suprathreshold contrasts would evoke the all-or-none burst. However, in tonic mode, the relay cell would be able to inform cortex about a large range of contrasts. In this regard, we predict that tonic firing would represent contrast in a much more linear fashion than would burst firing. There is support for this from receptive field studies of cells in the cat's lateral geniculate nucleus because there is considerably more response linearity in tonic than in burst firing (Guido et al. 1992, 1995; Sherman 1996). Also, the conclusion that burst firing is largely like an on-off switch—there is no response at all for subthreshold stimuli and a nearly fixed response for all suprathreshold stimuli—while tonic firing involves graded responses would suggest that a burst response would more clearly signal the presence of or change in a stimulus than would tonic firing. This, too, has been shown with in vivo studies because burst firing is better for signaling the detection of a novel or changed stimulus than is tonic firing (Guido et al. 1995; Sherman 1996).

Although our data indicate that burst firing would produce a similar response for a wide range of amplitudes of activating ESPSs, this happens only when the amount of deinactivation, or $h_T$, is the same. Our data also indicate that the amount of deinactivation does have an effect on the size of the $Ca^{2+}$ spike (Fig. 7). However, over a large range of initial membrane potentials, the effect is small. There is thus little effect on the number of action potentials activated (Fig. 3) and thus the signal relayed to cortex. During in vivo recording in both anesthetized and awake preparations (Guido and Weyand 1995; Guido et al. 1992), geniculate relay cells switch between burst and tonic firing, presumably under the control of inputs from cortex and brain stem that modulate membrane potential and thus the level of deinactivation (Lu et al. 1993; McCormick 1992; Sherman 1996; Sherman and Guillery 1996). Thus for the cell to begin firing in burst mode, there must first be a prolonged hyperpolarization, which may occur passively from the withdrawal of excitatory inputs or actively from inhibitory inputs, and the strength in terms of amplitude and duration of this hyperpolarization sets the extent of deinactivation. This, then, controls the amplitude of the burst response to the subsequent activating input to the relay cell. If the hyperpolarizing process that deinactivates these relay cells is fairly consistent in the behaving animal, leading to uniform deinactivation, then the response relayed to cortex in burst mode always would be fairly constant regardless of the stimulus; if this deinactivating process is variable, then so would responses in burst mode. At present, there are no published data on the variability in the amplitude of burst responses, nor do we understand these deinactivation processes well enough to predict this.

### *Latency of the $Ca^{2+}$ spike*

Although the intensity of the activating input has little effect on the amplitude of the burst response, it does affect the response latency, at least for smaller suprathreshold inputs (Figs. 8, *C* and *D*, and 9). The latency dependence comes from the interaction between the initial ohmic response and the voltage-dependent gating of $I_T$. According to voltage-clamp data, the activation gating of $I_T$ is sigmoidal, rising exponentially with voltage from zero to its half activation around −60 mV, with a ''width'' parameter of 6.2 mV. Conductance has an even steeper rise with

voltage because, in Hodgkin-Huxley-like descriptions, it depends on some power (2 in our model) of the activation variable, $m_T$, for the conductance of $I_T$. The activation gating is fast, but the activation level is so small (i.e., deactivated) in this low-voltage regime (even with inactivation removed) that when the ohmic depolarization enables recruitment of $I_T$ to begin, the growth of membrane voltage is very slow. For subthreshold inputs, the ohmic component (leakage plus injected current) becomes outward and dominates the weak $I_T$. Strong suprathreshold inputs mean that the voltage is more quickly brought into the range where the autocatalytic growth of $I_T$ occurs, and latency is short (as in Fig. 12). Over a narrow range of just suprathreshold depolarization, the competition between the ohmic and small inward $I_T$ means slow growth of membrane voltage until the nonlinear exponential rise of $I_T$ wins over the linear voltage dependence of leakage current. The latency is enhanced further because during the slow depolarization before initiation of the $Ca^{2+}$ spike, $I_T$ can inactivate somewhat (as seen in Fig. 9). A complementary account of these latency effects in a relay cell model is offered by Rose and Hindmarsh (1989) using the instantaneous *I-V* relation and phase plane concepts. Our explanations of latency do not invoke any opposing active $K^+$ currents, such as $I_A$. We have demonstrated in our model with $I_A$ blocked or with its inactivation slowed (see Fig. 10) that the long latency seen for just suprathreshold inputs is a property solely of $I_T$.

The implication of this seems obvious: the timing of responses relayed to cortex in burst mode must be very unreliable for near threshold stimuli. One prediction is that a cell firing in burst mode to low contrast stimuli would respond with a highly variable and long latency, but responses to high contrasts would show shorter latencies with less variation. How this latency behavior of burst firing for geniculate relay cells affects visual processing needs to be explored further. For instance, it is well known that it takes less time in psychophysical experiments to detect stimuli expected to evoke greater firing in retinal inputs, such as brighter stimuli (Alpern 1954; Lennie 1981; Wilson and Lit 1981) or stimuli with higher contrast (Harwerth and Levi 1978), and perhaps this property of burst firing contributes to this phenomenon.

### *Theoretical considerations on firing threshold for $Ca^{2+}$ spikes*

FitzHugh (1960, 1969) described two basic types of threshold behaviors in excitable membranes. A quasithreshold phenomenon is characterized by a finite latency and a continuous dependence of response amplitude on stimulus strength. In contrast, a singular-point threshold phenomenon exhibits infinite latency and a discontinuous stimulus-response curve. The latter type is associated with a steady-state current-voltage relation that is N-shaped as elaborated by Rinzel and Ermentrout (1989). The standard Hodgkin-Huxley model has the former type of excitability as does our minimal model. Comparison of these theoretical notions and our experimental data suggest that the relay cells that we observed also had the quasithreshold behavior, although with a very steep stimulus-response dependence. This means that one should in principle be able to evoke, using finely tuned stimuli, graded responses. Because of these rigorous distinctions we have throughout the paper referred to the relay cell's responsiveness as ''nearly'' all or none. If the continuous nature of the response amplitude is in question, it can sometimes be exposed by adjusting other stimulus or environmental parameters, such as the holding level of hyperpolarization for relay cells (as we have done in Fig. 11) or, for example, temperature in the Hodgkin-Huxley model and space-clamped squid giant axon (Cole et al. 1970; FitzHugh 1966).

Although our model is based on voltage-clamp data, it is idealized: for example, the cable properties of relay cells are ignored. Although relay cells are relatively compact electrotonically, we expect that some aspects of $Ca^{2+}$ spike generation are affected by the spatial distribution of T channels underlying $I_T$ and those for other intrinsic currents, as well as ionotropic and metabotropic receptors activated by various synaptic inputs. This deserves study. There is good evidence that much of $I_T$ is of dendritic origin (Destexhe et al. 1998; Munsch et al. 1997; Zhou et al. 1997). One expects that the membrane voltage versus current curves to be right-shifted if somatic inputs are delivered and $I_T$ is distally (i.e., largely dendritically) distributed (see Destexhe et al. 1998). Perhaps the additional time needed for recruitment when $I_T$ is remote might contribute to longer latencies as well.

It also would be useful to explore further with compartmental modeling the extent of $I_T$ recruitment that underlies variable latency responses. Our single compartment model shows reduced $I_T$ for longer latency responses (Fig. 8*A* and implied by Fig. 11 because $dV/dt$ is mostly due to $I_T$ during the upstroke of the $Ca^{2+}$ spike). If significant $Ca^{2+}$ entry is associated with burst mode the ability to grade, this entry could have functional significance. However, we see little suggestion of a graded $I_T$ in our experimental results (as interpreted in our experimental $dV/dt$ vs. $V$ plots, which have not been shown). It will be interesting to learn, with future modeling studies, why this is not seen. Perhaps the segregation of $I_T$ to distal sites away from our stimulating electrode ensures more autonomous burst responses and thus could explain as well the extreme lack of response amplitude dependence on stimulus in our experiments as compared with modest dependence in the theory.

### *Conclusions*

We have shown that activation of the $Ca^{2+}$ spike behaves qualitatively like that of conventional $Na^+/K^+$ action potentials, with a quasithreshold for voltage, a nearly all-or-none appearance, and a variable latency around threshold that drops precipitously with increasing intensity of activation. The major features of our experimental observations from current-clamp recording are supported by simulations in a reduced model based on voltage-clamp data. These properties of geniculate relay cells, which presumably extend generally to thalamic relay cells, have important implications for relay of information through thalamus to cortex.

One implication is that the relay of information during burst firing should be highly variable in time with near threshold stimuli but become much more stable with stronger activating inputs. Our results also suggest that when relay cells fire in burst mode as a result of being activated from hyperpolarized levels by their driving inputs, the response relayed to cortex is either zero, if the driving input is subthreshold, or a burst that is largely invariant in amplitude over a wide range of suprathreshold inputs. This contrasts sharply with tonic responsiveness when relay cells fire as a result of being activated from depolarized levels by their driving inputs: here the response relayed to cortex is graded over a large range of input inten-

sities. Thus a relay cell during burst firing is geared to signal rather dramatically the presence of or sudden change in its driving inputs (e.g., a novel visual stimulus in the receptive field of a geniculate relay cell), whereas during tonic firing it would more readily signal continuous changes in its driving inputs. This notion is consistent with a previous suggestion from receptive field studies that tonic firing of geniculate cells provides a more linear relay better adapted to analyzing a stimulus faithfully, whereas burst firing provides better stimulus detectability (Guido et al. 1995; Sherman 1996).

We are grateful to A. Houweling and T. Ozaki for sharing their NEURON scripts for the Huguenard-McCormick model.

This work was supported by National Eye Institute Grant EY-03038 and a postdoctoral research fellowship to X. J. Zhan from Fight for Sight, research division of Prevent Blindness America.

Address for reprint requests: S. M. Sherman, Dept. of Neurobiology, State University of New York, Stony Brook, NY 11794-5230.

Received 24 August 1998; accepted in final form 11 January 1999.

## REFERENCES

ALPERN, M. Relation of visual latency to intensity. *Arch. Ophthalmol.* 51: 369–374, 1954.

COLE, K. S., GUTTMAN, R., AND BEZANILLA, F. Nerve membrane excitation without threshold. *Proc. Natl. Acad. Sci. USA* 65: 884–891, 1970.

COULTER, D. A., HUGUENARD, J. R., AND PRINCE, D. A. Calcium currents in rat thalamocortical relay neurones: kinetic properties of the transient, low-threshold current. *J. Physiol. (Lond.)* 414: 587–604, 1989.

CRUNELLI, V., KELLY, J. S., LERESCHE, N., AND PIRCHIO, M. The ventral and dorsal lateral geniculate nucleus of the rat: intracellular recordings in vitro. *J. Physiol. (Lond.)* 384: 587–601, 1987.

CRUNELLI, V., LIGHTOWLER, S., AND POLLARD, C. E. A T-type $Ca^{2+}$ current underlies low-threshold $Ca^{2+}$ potentials in cells of the cat and rat lateral geniculate nucleus. *J. Physiol. (Lond.)* 413: 543–561, 1989.

DESTEXHE, A., NEUBIG, M., ULRICH, D., AND HUGUENARD, J. Dendritic low-threshold calcium currents in thalamic relay cells. *J. Neurosci.* 18: 3574–3588, 1998.

FITZHUGH, R. Thresholds and plateaus in the Hodgkin-Huxley nerve equations. *J. Gen. Physiol.* 43: 867–896, 1960.

FITZHUGH, R. Theoretical effect of temperature on threshold in the Hodgkin-Huxley nerve model. *J. Gen. Physiol.* 49: 989–1005, 1966.

FITZHUGH, R. Mathematical models for excitation and propagation in nerve. In: *Biological Engineering,* edited by H. P. Schwan. New York: McGraw-Hill, 1969, p. 1–84.

FRIEDLANDER, M. J., LIN, C.-S., STANFORD, L. R., AND SHERMAN, S. M. Morphology of functionally identified neurons in lateral geniculate nucleus of the cat. *J. Neurophysiol.* 46: 80–129, 1981.

GHAZANFAR, A. A. AND NICOLELIS, M. A. Nonlinear processing of tactile information in the thalamocortical loop. *J. Neurophysiol.* 78: 506–510, 1997.

GUIDO, W., LU, S.-M., AND SHERMAN, S. M. Relative contributions of burst and tonic responses to the receptive field properties of lateral geniculate neurons in the cat. *J. Neurophysiol.* 68: 2199–2211, 1992.

GUIDO, W., LU, S.-M., VAUGHAN, J. W., GODWIN, D. W., AND SHERMAN, S. M. Receiver operating characteristic (ROC) analysis of neurons in the cat's lateral geniculate nucleus during tonic and burst response mode. *Vis. Neurosci.* 12: 723–741, 1995.

GUIDO, W. AND WEYAND, T. Burst responses in thalamic relay cells of the awake behaving cat. *J. Neurophysiol.* 74: 1782–1786, 1995.

GUILLERY, R. W. A study of Golgi preparations from the dorsal lateral geniculate nuceleus of the adult cat. *J. Comp. Neurol.* 128: 21–50, 1966.

HARWERTH, R. S. AND LEVI, D. M. Reaction time as a measure of suprathreshold grating detection. *Vision Res.* 18: 1579–1586, 1978.

HERNÁNDEZ-CRUZ, A. AND PAPE, H.-C. Identification of two calcium currents in acutely dissociated neurons from the rat lateral geniculate nucleus. *J. Neurophysiol.* 61: 1270–1283, 1989.

HILLE, B. *Ionic Channels of Excitable Membranes.* Sunderland, MA: Sinauer Associates, 1992.

HUGUENARD, J. R. AND MCCORMICK, D. A. Simulation of the currents involved in rhythmic oscillations in thalamic relay neurons. *J. Neurophysiol.* 68: 1373–1383, 1992.

HUGUENARD, J. R. AND MCCORMICK, D. A. *Electrophysiology of the Neuron.* New York: Oxford, 1994.

JAHNSEN, H. AND LLINÁS, R. Electrophysiological properties of guinea-pig thalamic neurones: an in vitro study. *J. Physiol. (Lond.)* 349: 205–226, 1984a.

JAHNSEN, H. AND LLINÁS, R. Ionic basis for the electroresponsiveness and oscillatory properties of guinea-pig thalamic neurones in vitro. *J. Physiol. (Lond.)* 349: 227–247, 1984b.

LENNIE, P. The physiological basis of variations in visual latency. *Vision Res.* 21: 815–824, 1981.

LU, S.-M., GUIDO, W., AND SHERMAN, S. M. The brainstem parabrachial region controls mode of response to visual stimulation of neurons in the cat's lateral geniculate nucleus. *Vis. Neurosci.* 10: 631–642, 1993.

MCCORMICK, D. A. Functional properties of a slowly inactivating potassium current in guinea pig dorsal lateral geniculate relay neurons. *J. Neurophysiol.* 66: 1176–1189, 1991.

MCCORMICK, D. A. Neurotransmitter actions in the thalamus and cerebral cortex and their role in neuromodulation of thalamocortical activity. *Prog. Neurobiol.* 39: 337–388, 1992.

MCCORMICK, D. A. AND HUGUENARD, J. R. A model of the electrophysiological properties of thalamocortical relay neurons. *J. Neurophysiol.* 68: 1384–1400, 1992.

MUNSCH, T., BUDDE, T., AND PAPE, H. C. Voltage-activated intracellular calcium transients in thalamic relay cells and interneurons. *Neuroreport* 8: 2411–2418, 1997.

RINZEL, J. AND ERMENTROUT, B. Analysis of neural excitability and oscillation. In: *Methods in Neuronal Modeling,* edited by C. Koch and I. Segev. Cambridge, MA: MIT Press, 1989, p. 135–169.

ROGAWSKI, M. A. The A-current: how ubiquitous a feature of excitable cells is it? *Trends Neurosci.* 8: 214–219, 1985.

ROSE, R. M. AND HINDMARSH, J. L. The assembly of ionic currents in a thalamic neuron. II. The stability and state diagrams. *Proc. R. Soc. Lond. B Biol. Sci.* 237: 289–312, 1989.

SHERMAN, S. M. Dual response modes in lateral geniculate neurons: mechanisms and functions. *Vis. Neurosci.* 13: 205–213, 1996.

SHERMAN, S. M. AND FRIEDLANDER, M. J. Identification of X versus Y properties for interneurons in the A-laminae of the cat's lateral geniculate nucleus. *Exp. Brain Res.* 73: 384–392, 1988.

SHERMAN, S. M. AND GUILLERY, R. W. The functional organization of thalamocortical relays. *J. Neurophysiol.* 76: 1367–1395, 1996.

STERIADE, M. AND LLINÁS, R. The functional states of the thalamus and the associated neuronal interplay. *Physiol. Rev.* 68: 649–742, 1988.

STORM, J. F. Temporal integration by a slowly inactivating K current in hippocampal neurons. *Nature* 336: 379–381, 1988.

TROY, J. B. AND ENROTH-CUGELL, C. X and Y ganglion cells inform the cat's brain about contrast in the retinal image. *Exp. Brain Res.* 93: 383–390, 1993.

WANG, X.-J., RINZEL, J., AND ROGAWSKI, M. A. A model of the T-Type calcium current and the low-threshold spike in thalamic neurons. *J. Neurophysiol.* 66: 839–850, 1991.

WILLIAMS, S. R., TÓTH, T. I., TURNER, J. P., HUGHES, S. W., AND CRUNELLI, V. The ''window'' component of the low threshold $Ca^{2+}$ current produces input signal amplification and bistability in cat and rat thalamocortical neurones. *J. Physiol. (Lond.)* 505: 689–705, 1997.

WILSON, A. J. AND LIT, A. Effects of photopic annulus luminance level on reaction time and on the latency of evoked cortical potential responses to target flashes. *J. Opt. Soc. Am.* 71: 1481–1486, 1981.

ZHAN, X. J. AND TROY, J. B. An efficient method that reveals both the dendrites and the soma mosaics of retinal ganglion cells. *J. Neurosci. Methods* 72: 109–116, 1997.

ZHOU, Q., GODWIN, D. W., O'MALLEY, D. M., AND ADAMS, P. R. Visualization of calcium influx through channels that shape size burst and tonic firing modes of thalamic relay cells. *J. Neurophysiol.* 77: 2816–2825, 1997.